Inorganic Chemistry

Article

pubs.acs.org/IC

An Efficient, Thermally Stable Cerium-Based Silicate Phosphor for Solid State White Lighting

Jakoah Brgoch,*[,†] Christopher K. H. Borg,[†] Kristin A. Denault,[†,§] Alexander Mikhailovsky,[‡] Steven P. DenBaars,[†,§] and Ram Seshadri[†,§]

[†]Solid State Lighting and Energy Center, University of California, Santa Barbara, Santa Barbara, California 93106, United States

[‡]Department of Chemistry and Biochemistry, University of California, Santa Barbara, Santa Barbara, California 93106, United States

[§]Materials Department, University of California, Santa Barbara, Santa Barbara, California 93106, United States

Supporting Information

ABSTRACT: A novel cerium-substituted, barium yttrium silicate has been identified as an efficient blue-green phosphor for application in solid state lighting. $Ba_9Y_2Si_6O_{24}:Ce^{3+}$ was prepared and structurally characterized using synchrotron X-ray powder diffraction. The photoluminescent characterization identified a major peak at 394 nm in the excitation spectrum, making this material viable for near-UV LED excitation. An efficient emission, with a quantum yield of ≈60%, covers a broad portion (430−675 nm) of the visible spectrum, leading to the blue-green color. Concentration quenching occurs when the Ce^{3+} content exceeds ≈3 mol %, whereas high temperature photoluminescent measurements show a 25% drop from the room temperature efficiency at 500 K. The emission of this compound can be red-shifted via the solid solution $Ba_9(Y_{1-y}Sc_y)_{1.94}Ce_{0.06}Si_6O_{24}$ (y = 0.1, 0.2), allowing for tunable color properties when device integration is considered.

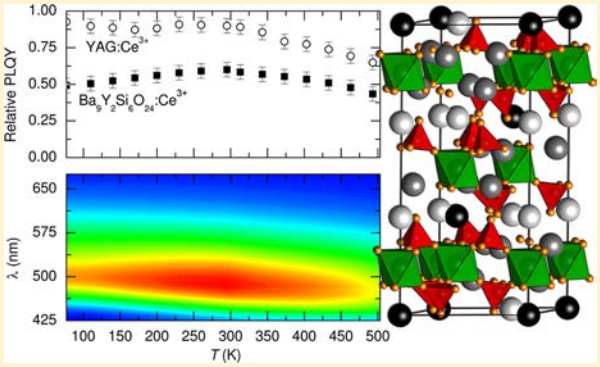

INTRODUCTION

Improvements in the efficiency of light emitting diodes (LEDs) have provided a means of increasing energy savings by replacing traditional incandescent bulbs with an alternative lighting source. The most common method of producing white light from a monochromatic LED is by using an inorganic phosphor that partially down-converts the blue or near-UV emission produced by an (In)GaN LED to a yellow-red emission.[1] The combination of the partially transmitted blue light and yellow-red phosphor emission appears as a white light. Currently, the most common phosphor for this application is cerium-substituted yttrium aluminum garnet ($YAG:Ce^{3+}$).[1−3] When Ce^{3+} is substituted for Y^{3+} in $YAG:Ce^{3+}$, the coordination environment leads to a strong crystal field splitting of the virtual Ce 5d orbitals. This, in turn, shifts the Ce^{3+} 5d to 4f orbital transition into the yellow region of the visible spectrum. However, $YAG:Ce^{3+}$ has a few major drawbacks such as low thermal stability at high temperatures and the lack of a red component that leads to a less desirable "cool" white light.[2,4]

The search for new phosphors with remarkable optical properties has recently focused on compounds that form complex solid solutions, providing a mechanism to tune the luminescent properties. For instance, in the orthosilicate series $(M_{1-x}M'_x)_2SiO_4:Eu^{2+}$ (M/M′ = Mg, Ca, Sr, Ba), the emission color can be tuned from violet to red-orange and the thermal stability modified depending on the M/M′ components and their respective ratios.[5,6] In the orthosilicates, the modification of optical properties originate from changes in the unit cell volume and corresponding M/M′−O bond distances. A larger unit cell and longer M/M′−O bond distances give weaker crystal field splitting, which blue-shifts the emission. Structural distortion can also be a mechanism to tune the optical properties.[7,8] In the series $Sr_2Ba(AlO_4F)_{1-x}(SiO_5)_x:Ce^{3+}$, increasing x causes an increase in the unit cell volume. Contrary to the previous example, the emission in this series red-shifts. Here, increasing x causes a distortion in the Ce^{3+} coordination environment that leads to an increasing crystal field splitting and the observed change in optical properties.[7] Another silicate solid solution that shows tunable emission properties is the compound $(Ba_{1-\delta}Sr_\delta)_9Sc_2Si_6O_{24}:RE$ (RE = Eu^{2+}, Ce^{3+}).[9−11] When Eu^{2+} is substituted for Ba in the Ba end-member host, an emission peak emerges at $\lambda_{max} \approx 500$ nm, giving rise to a green phosphor. The quantum yield of emission for this compound is ≈45%.[10] The emission can be red-shifted by nearly 20 nm through a decrease in the unit cell volume going from Ba-rich to Sr-rich in the solid solution.[10] Using Ce^{3+} as the activator ion yields a UV-excited phosphor that emits in

Received: March 12, 2013
Revised: June 9, 2013
Accepted: June 21, 2013
Published: July 3, 2013

   dx.doi.org/10.1021/ic400614r | Inorg. Chem. 2013, 52, 8010−8016

the near-UV to blue. The quantum yield of this process is about half (≈20%) that of Eu^{2+} phosphor.[11] Because Ce^{3+} is much smaller (r = 1.196 Å; 9-coordinated) than Ba $^{2+}$ (1.47 Å; 9-coordinated), there is a large potential for nonradiative relaxation. Substituting the smaller Sr^{2+} (1.31 Å; 9-coordinated) ion improves the quantum yield slightly, though it is still rather low. Clearly, the alkaline earth site in this structure type is not ideal for the occupation of a luminescent center. The structure does contain a ScO_6 pseudo-octahedral site that would be ideal for rare-earth occupation, in particular Ce^{3+}. Unfortunately, the polyhedral volume is too small for substitution to occur.

Herein, we report the preparation of the yttrium analogue, $Ba_9Y_2Si_6O_{24}:Ce^{3+}$, as an efficient near-UV to blue-green phosphor. The structure was determined using synchrotron X-ray diffraction, and the Ce^{3+} content was optimized. The optical properties examined include determining the photoluminescent quantum yield (PLQY), the Commission Internationale de L'éclairage (CIE) color coordinates, and the critical distance for energy transfer, and these are all reported. Additionally, the temperature dependence of the optical properties for $Ba_9Y_2Si_6O_{24}$ is investigated, and we showed the efficiency was maintained even at high temperatures (>500 K). Finally, a solid solution of $Ba_9(Y_{1-y}Sc_y)_2Si_6O_{24}:Ce^{3+}$ (y = 0.05, 0.1, ..., 0.25) is employed to tune the emission color from blue-green to green based on changes in the polyhedral volume.

EXPERIMENTAL PROCEDURE

Sample Preparation. Polycrystalline samples of $Ba_9(Y_{1-x}Ce_x)_2Si_6O_{24}$ (x = 0, 0.01, 0.03, ..., 0.09, 0.12) and $Ba_9(Y_{1-y}Sc_y)_{1.94}Ce_{0.06}Si_6O_{24}$ (y = 0.05, 0.1, ..., 0.25) were prepared by the conventional high temperature solid state reaction. The starting materials ($BaCO_3$, Cerac, 99.9%; Y_2O_3, Cerac, 99.99%; Sc_2O_3, Stanford Materials Corporation, 99.99%; SiO_2, Johnson-Matthey, 99.9%; CeO_2, Cerac, 99.9%) were all weighed out in the desired stoichiometry and thoroughly mixed using an agate mortar and pestle for 30 min. The mixed powders were pressed into a pellet and placed in an alumina crucible (CoorsTek) with sacrificial powder to prevent contact between the pellet and the crucible. The mixtures were fired in a tube furnace under reducing atmosphere (95% N_2/5% H_2) at 1350 °C for 4 h with heating and cooling rates of 3 °C/min. Additionally, a sample of $Ba_{1.94}Ce_{0.06}SiO_4$ was prepared using the same starting materials at 1400 °C for 8 h to ensure the optical properties observed here are not from the impurity in the desired phase. The products are all colorless powders. Each mixture was subsequently ground to a fine powder with an agate mortar and pestle for further analysis.

Structural and Optical Properties. High resolution synchrotron X-ray powder diffraction data were collected for $Ba_9Y_2Si_6O_{24}$, $Ba_9Y_{1.94}Ce_{0.06}Si_6O_{24}$, and $Ba_9(Y_{1-y}Sc_y)Si_6O_{24}$ (y = 0.1, 0.2) at room temperature using beamline 11-BM at the Advanced Photon Source. The average wavelength was 0.413 949 Å. The diffraction data were fit by Rietveld refinements using the general structure analysis system (GSAS).[12,13] The background was handled using a shifted Chebyshev function, whereas the peak shapes were handled using a pseudo-Voigt function with Finger−Cox−Jephcoat asymmetry to correct for axial divergence at low angles. Scanning electron microscopy (SEM) images were collected using a FEI XL40 Sirion FEG digital scanning microscope. Because the samples are highly insulating, the surface was sputtered with gold to limit charging and a low (5.00 kV) accelerating voltage was used. The images were collected using the resulting secondary electrons.

Room temperature and low temperature photoluminescence spectra were obtained on a Perkin-Elmer LS55 spectrophotometer. Each sample was mixed thoroughly with KBr (≥99%, FT-IR grade, Sigma-Aldrich; ≈10:1 KBr/sample ratio by mass). The samples were pressed into a pellet (13 mm) for the room temperature measurements and used as a packed powder in a quartz tube for low temperature measurements. High temperature emission data were collected from room temperature to 503 K using a home-built fluorometer incorporating a heating stage and an excitation wavelength of 405 nm. For the PLQY measurements, the phosphor powders were encapsulated in silicone resin (GE Silicones, RTV615) and deposited on a quartz substrate (Chemglass). The samples were then placed in a Spectralon-coated integrating sphere (6 in. diameter, Lab-sphere) and excited using 405 nm light generated by a solid state laser (Crystalaser DL-405-40-S) operated at a power between 1 and 2 mW. The light was collected by a quartz lens and directed onto a calibrated Si photodiode (Newport 818-UV) using filters (Omega Filters) to collect respective wavelengths. Additional experimental details have been described previously.[14,15]

The CIE chromaticity coordinates were determined using an Instrument Systems integrating sphere (ISP-500) with a MAS-40 CCD array spectrometer and the SpecWin Lite software. The samples were excited using a commercially available laser diode (Pioneer, BDR-SO6J) with an emission $\lambda_{max} \approx$ 402 nm and a forward bias current of 20 mA.

RESULTS AND DISCUSSION

Structural Determination of $Ba_9Y_2Si_6O_{24}$. $Ba_9Y_2Si_6O_{24}$, illustrated in Figure 1, is a novel silicate compound and was prepared as the major phase (as indicated by powder X-ray diffraction) with only a minor impurity of Ba_2SiO_4. All attempts to remove the silicate impurity, including varying the loaded stoichiometry and reaction heating profile, proved unsuccessful. The concentration of the impurity was limited by thoroughly mixing the starting materials using acetone as a grinding medium and following the heating profile described in the Experimental Procedure section.

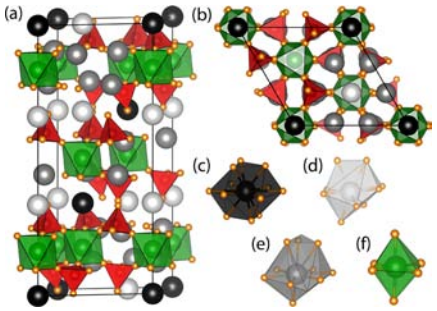

Figure 1. Structure of $Ba_9Y_2Si_6O_{24}$ projected along (a) the [100] direction and (b) the [001] direction. The oxygen polyhedra around (c) Ba1, (d) Ba2, (e) Ba3, and (f) Y.

The as-ground sample was imaged using the secondary electrons produced by a SEM, Figure 2, to determine the particle morphology, size, and size distribution. As is evident from the micrographs, the particles have a wide dispersion of

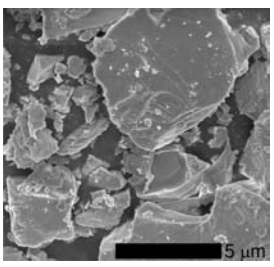

Figure 2. Sample imaged by the SEM secondary electrons showing a wide range of particle size, including agglomerates of the smaller particles.

dx.doi.org/10.1021/ic400614r | Inorg. Chem. 2013, 52, 8010−8016

sizes that are generally smaller than ≈10 μm and various morphologies. The $Ba_9Y_2Si_6O_{24}$ structure crystallizes in the $Ba_9Sc_2Si_6O_{24}$ structure type[16] and was refined from this starting point using the Rietveld method with high resolution synchrotron X-ray powder diffraction data. Details of the refinement are presented in Tables 1 and 2, and the refined X-ray pattern is presented in Figure 3. $Ba_9Y_2Si_6O_{24}$ crystallizes in rhombohedral space group $R\bar{3}$ (No. 148) with lattice parameters of a = 10.02892(1) Å and c = 22.16790(4) Å. It is composed of distorted, isolated SiO_4 tetrahedral units similar to those of the orthosilicates (e.g., M_2SiO_4). However, in this structure, the tetrahedra are corner-shared with YO_6 distorted octahedra (Figure 1f). Each YO_6 unit is connected via two tetrahedral units, creating tetrahedral−octahedral−tetrahedral layers that stack along the [001] direction forming two-dimensional sheets. The SiO_4 tetrahedra are distorted, with Si−O bond distances between 1.586(5) and 1.669(5) Å and O−Si−O angles ranging between 105.9(4) and 117.9(3)°. Similarly, the YO_6 octahedra have two different bond distances of 2.190(7) and 2.255(6) Å with O−Y−O bond angles distorted away from 90°, ranging between 83.2(3)° and 97.1(3)° . The structure also contains three independent Ba^{2+} sites. Ba1 occupies Wyckoff position 3*a* with a 3-fold inversion symmetry. It sits in between the two-dimensional sheets and is coordinated by 12 oxygen atoms that form a distorted cubeoctahedron, as shown in Figure 1c. The six oxygen atoms surrounding the waist (Ba1−O1) have a bond distance of 3.321(6) Å, whereas the remaining six oxygen atoms have shorter bond distances of 2.849(6) Å. Ba2, Figure 1d, occupies Wyckoff site 6*c* and is coordinated to 9 oxygen atoms in a distorted, tricapped trigonal prism. Ba3, Figure 1e, sits at a general position (Wyckoff site 18*f*) and is connected to 10 oxygen atoms. The bond distances for additional selected interatomic bonds are presented in Table 3.

Table 1. Rietveld Refinement and Crystal Data for $Ba_9Y_2Si_6O_{24}$

formula	$Ba_9Y_2Si_6O_{24}$
radiation type, λ (Å)	synchrotron (11-BM), 0.413 95
2θ range (deg)	0.5−49.995
temperature (K)	295
crystal system	trigonal
space group; Z	$R\bar{3}$; 3
lattice parameters (Å)	a = 10.02892(1)
	c = 22.16790(4)
volume (Å^3)	V = 1930.92(1)
R_p	10.3
R_{wp}	12.9
R_f^2	7.4
χ^2	7.39

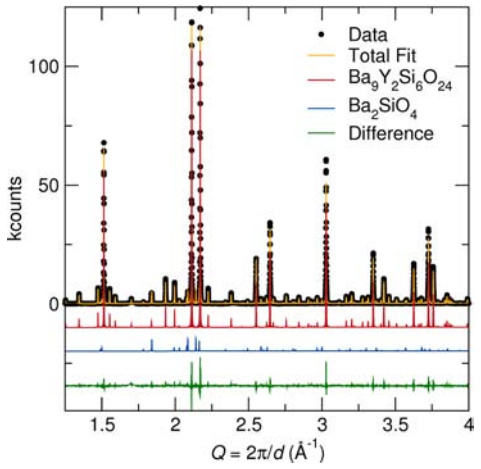

Figure 3. Synchrotron X-ray diffraction pattern of $Ba_9Y_2Si_6O_{24}$. The pattern contains two phases: $Ba_9Y_2Si_6O_{24}$ (red) and Ba_2SiO_4 (blue).

Table 3. Selected Interatomic Distances for $Ba_9Y_2Si_6O_{24}$

atom	distance (Å)	atom	distance (Å)
Ba1−O1 (6×)	3.321(6)	Ba1−O3 (6×)	2.849(6)
Ba2−O1 (3×)	2.907(5)	Ba2−O2 (3×)	3.119(8)
Ba2−O4 (3×)	2.774(6)	Ba3−O2	3.094(8)
Ba3−O1	2.535(5)	Ba3−O2	2.983(6)
Ba3−O2	3.107(6)	Ba3−O3	3.059(1)
Ba3−O4	2.710(6)	Ba3−O4	2.718(6)
Si−O1	1.586(5)	Ba3−O4	3.115(6)
Si−O2	1.669(5)	Y−O2 (3×)	2.190(7)
Si−O3	1.649(1)	Y−O3 (3×)	2.255(6)
Si−O4	1.634(8)		

Optical Properties of $Ba_9Y_2Si_6O_{24}:Ce^{3+}$. To prepare the phosphor, Ce^{3+} (the luminescent center) is substituted for Y^{3+} following the composition $Ba_9(Y_{1-x}Ce_x)Si_6O_{24}$ (x = 0, 0.01, 0.03, ..., 0.09, 0.12). Because Ce^{3+} (1.01 Å; 6-coordinated) is larger than Y^{3+} (0.900 Å; 6-coordinated), the lattice parameters should increase with substitution.[17] As shown in Figure 4a, the lattice parameters actually decrease upon substitution. This

Table 2. Refined Atomic Coordinates and Equivalent Isotropic Displacement Parameters of $Ba_9Y_2Si_6O_{24}$ As Determined by Rietveld Refinement of Powder Synchrotron X-Ray Diffraction Data Collected at Room Temperature[a]

atom	Wyckoff position	x	y	z	U_{eq}
Ba1	3*a*	0	0	0	21.8(4)
Ba2	6*c*	1/3	2/3	0.00394(5)	13.9(2)
Ba3	18*f*	0.02994(5)	0.66953(8)	0.10891(3)	9.9(1)
Y	6*c*	0	0	0.16481(6)	3.9(3)
Si	18*f*	0.3373(3)	0.01966(2)	0.07338(18)	2.8(4)
O1	18*f*	0.3592(5)	0.0664(5)	0.0042(2)	8.2(5)
O2	18*f*	0.4853(7)	0.1586(7)	0.1114(3)	8.2(5)
O3	18*f*	−0.009(1)	0.1702(7)	0.1011(2)	8.2(5)
O4	18*f*	0.1380(7)	0.4740(7)	0.0932(2)	8.2(5)

[a]Atomic mixing of Ce^{3+} was not considered in the model due to its small concentration (3%). U_{eq} is defined as one-third of the trace of the orthogonalized U^{ij} tensor (×10^{-3}, Å^2).

dx.doi.org/10.1021/ic400614r | Inorg. Chem. 2013, 52, 8010−8016

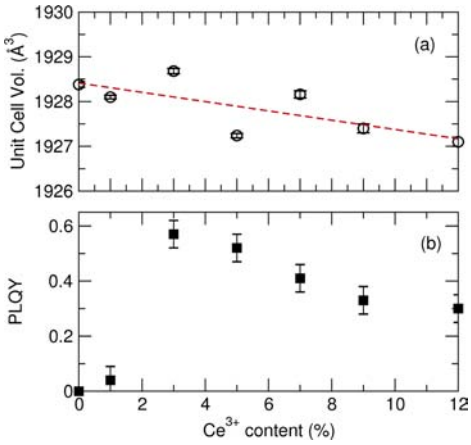

Figure 4. (a) Unit cell volume determined for the compounds $Ba_9(Y_{1-x}Ce_x)_2Si_6O_{24}$ (x = 0, 0.01, 0.03, 0.05, 0.07, 0.09, 0.12) using a LeBail fit. (b) The optimum Ce^{3+} content was determined by varying the Ce content and measuring the PLQYs excited at 405 nm. Standard error for the PLQY measurements are ±5%.

discrepancy likely stems from Ce^{3+} occupying the Ba^{2+} sites as well as the Y^{3+} site. Because Ce^{3+} (1.196 Å; 9-coordinated) is much smaller than Ba^{2+} (1.47 Å; 9-coordinated), substitution at the Ba^{2+} and Y^{3+} sites could lead to the anomalous behavior observed here. Attempts to refine the occupation of Ce^{3+} in the Rietveld refinement of the synchrotron X-ray powder diffraction data were unsuccessful. For instance, placing Ce^{3+} on the Y^{3+} site led to a nonphysical, negative occupancy of Ce^{3+} at the site and therefore was not considered in the refinement. Nevertheless, the observed U_{eq} for Y^{3+} without Ce^{3+} is slightly smaller (Supporting Information) than expected, indicating Ce^{3+} has likely substituted. Further analysis of the thermal parameters revealed a wide range of U_{eq} values for the Ba^{2+} sites (8×10^3 to 17×10^3 Å^2), further suggesting the possibility of Ba^{2+}/Ce^{3+} mixing. Although Ce^{3+}/Y^{3+} mixing could not be explicitly refined from the X-ray diffraction data, the optical properties confirm the presence of the substitution. Previously, the optical characterization of cerium-substituted $Ba_9Sc_2Si_6O_{24}:Ce^{3+}$ showed three excitation peaks from the presence of Ce^{3+} on the Ba^{2+} sites.[11] However, as discussed below, four peaks are present in $Ba_9Y_2Si_6O_{24}:Ce^{3+}$. The only structural difference between these two compounds is the presence of a ScO_6 versus YO_6 octahedral unit. Because Y^{3+} is closer in size to Ce^{3+} than to Sc^{3+}, it follows that Ce^{3+} can substitute in the YO_6 but not the ScO_6 octahedra. The preparation of a Y−Sc solid solution, which is discussed in the final section of this paper, shows the evolution of the fourth peak as a function of the Y/Sc content, further illustrating the dependence of the octahedral site composition.

As Figure 4b illustrates, the PLQY (excited at 405 nm) increases slightly with a 1% Ce^{3+} substitution followed by a dramatic increase to a maximum PLQY of 57% at 3% Ce^{3+} substitution. Additional Ce^{3+} decreases the quantum yield because of concentration quenching effects arising from an energy transfer from one luminescent center to another. The critical distance of this energy transfer process (R_c) can be calculated using eq 1, where V is the unit cell volume, x_c is the critical Ce^{3+} concentration, and N is the number of lattice sites in the unit cell that can be occupied by activator ions (the Wyckoff multiplicity of the activator sites).[18]

$$R_c \approx 2\left[\frac{3V}{4\pi x_c N}\right]^{1/3} \quad (1)$$

In $Ba_9Y_2Si_6O_{24}:Ce^{3+}$, x_c = 0.03 and V = 1928.68(6) Å^3. The number of Ce^{3+} sites in the unit cell has a range between N = 6 and 33 depending on the substitution of Ce^{3+} on the Ba^{2+} sites. Using these values, the resulting critical energy transfer distance ranges between 7.1 and 12.7 Å. These quenching distances are similar to those determined in other phosphors; $CaMgSi_2O_6:Eu^{2+}$ [19] has a critical distance of 12 Å, $Ba_2ZnSi_2O_7:Eu^{2+}$ has an R_c of 19 Å,[20] and the industry standard phosphor $YAG:Ce^{3+}$ has an R_c of 16 to 18 Å.

The room temperature (298 K) and low temperature (77 K) excitation and emission spectra of $Ba_9Y_{1.94}Ce_{0.06}Si_6O_{24}$ are presented in parts a and b of Figure 5, respectively. The 298 K

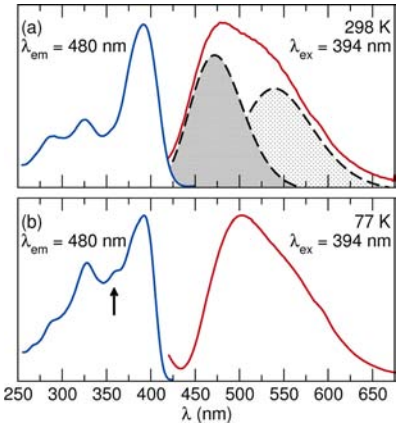

Figure 5. (a) Room temperature (298 K) and (b) low temperature (77 K) excitation (λ_{em} = 480 nm) and emission (λ_{ex} = 394 nm) spectra of $Ba_9Y_{1.94}Ce_{0.06}Si_6O_{24}$. The emission peak is fit by two Gaussian curves separated by 2600 cm^{-1}.

excitation spectra, collected using λ_{em} = 480 nm, extends from 250 to 420 nm and contains three peaks. The two highest energy (shortest wavelength) peaks are attributed to Ce^{3+} occupying the Ba^{2+} site because these peaks occur in nearly the same energy range as in the scandium series, $Ba_9Sc_2Si_6O_{24}:Ce^{3+},Li^+$.[11] Although the scandium series contains three peaks arising from the three independent Ba^{2+} sites, only two peaks are observed in the room temperature data. The low temperature excitation spectra reveal the third peak (highlighted by an arrow in Figure 5b), completing the three expected peaks from the Ba^{2+} sites. The main excitation peak occurs at λ_{max} = 394 nm from Ce^{3+} occupying the pseudo-octahedral coordination of the Y^{3+} site. This peak is not observed in $Ba_9Sc_2Si_6O_{24}:Ce^{3+},Li^+$ because the ScO_6 octahedral volume (12.43 Å^3) is too small for the Ce^{3+} ion. Here, the YO_6 octahedral volume is 15% larger (14.66 Å^3), affording enough room for Ce^{3+} substitution. Despite the volume increase, Ce^{3+} is still too large for the YO_6 octahedra, resulting in short Ce−O bonds. As illustrated in eq 2, the crystal field splitting, Δ, is inversely related to the bond distance, R, where Z is the anionic charge, e is the charge of the electron, and r is the radius of the 5d wave functions.[21]

$$\Delta = \frac{Ze^2r^4}{6R^5} \quad (2)$$

dx.doi.org/10.1021/ic400614r | Inorg. Chem. 2013, 52, 8010−8016

This clearly illustrates that the longer wavelength position of the excitation band centered at 394 nm emerges from squeezing Ce^{3+} on the smaller yttrium site, whereas the shorter wavelength peaks stem from Ce^{3+} sitting on the larger Ba^{2+} sites.

The emission spectra, collected using λ_{ex} = 394 nm, is broad, extending from 400 to 675 nm. This data can be fit by two Gaussian curves separated by approximately 2600 cm^{-1} corresponding to the spin−orbit-assisted $^2D_{3/2}$ to $^2F_{5/2}$ and $^2F_{7/2}$ transitions.[22] The position of the emission λ_{max} for this system does not appear to be dependent on the concentration of Ce^{3+} substitution. As a note, the excitation of $Ba_{1.94}Ce_{0.06}SiO_4$ at 394 nm did not yield an emission signal, confirming the observed luminescent properties are from the desired phase. When $Ba_{1.94}Ce_{0.06}SiO_4$ was excited at 351 nm, a PLQY ≈50% resulted. From the 298 K emission spectra, the CIE chromaticity coordinates, illustrated in Figure 6, are determined to be (0.241, 0.339), giving a blue-green emission.

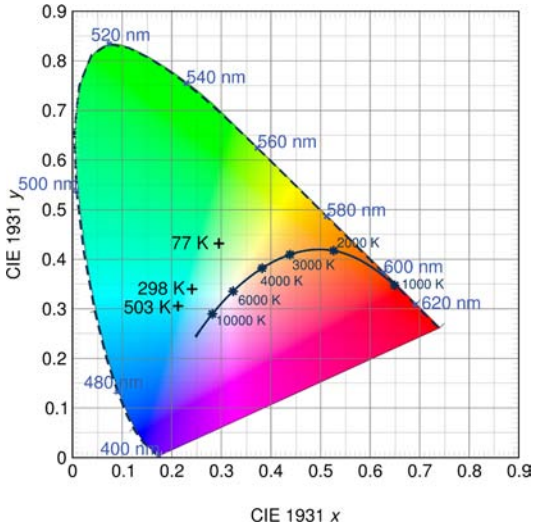

Figure 6. CIE color coordinates of $Ba_9Y_{1.94}Ce_{0.06}Si_6O_{24}$ at low temperature (77 K), room temperature (298 K), and high temperature (503 K) showing the true color of the phosphor, taking into account the broad emission spectra.

The temperature dependence of the quantum yield was also determined for $Ba_9Y_2Si_6O_{24}:Ce^{3+}$ and compared to that of the standard YAG:Ce^{3+}. In YAG:Ce^{3+}, the emission intensity approaches 100% below room temperature and is relatively constant. The room temperature PLQY is ≈90%, which is in agreement with the measurements taken from the integrating sphere. For $Ba_9Y_2Si_6O_{24}:Ce^{3+}$, the relative PLQY as a function of temperature was determined by comparing the integrated intensities against the largest peak (at 295 K) and then scaled by the room temperature PLQY determined from the integrating sphere (57%). Interestingly, the relative PLQY decreases with decreasing temperature, dropping by nearly 20% by 77 K. Although this anomaly has been observed in systems that contain an energy transfer process,[23] the mechanism in this system is unclear and requires further investigation. At 77 K, emission spectra are red-shifted by approximately 20 nm from the room temperature data. This shift in emission wavelength causes the CIE coordinates to strongly red-shift to (0.285, 0.442), giving a more green emission. This change follows a contraction of the lattice parameters (and bond distances) at low temperature, again leading to stronger crystal field splitting and the observed red shift.

High temperature quenching studies of $Ba_9Y_{1.94}Ce_{0.06}Si_6O_{24}$ show the phosphor has excellent quenching characteristics. The relative PLQY, shown in Figure 7a, decreases by only 25% of

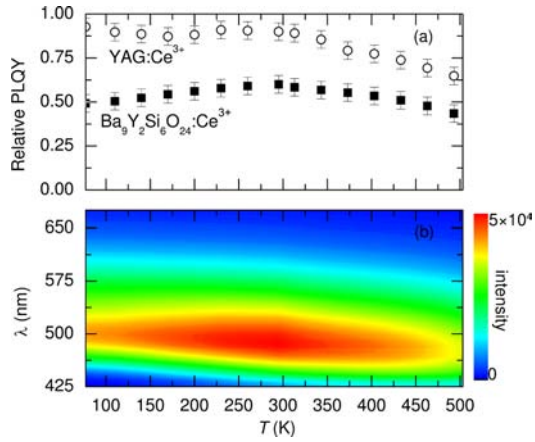

Figure 7. (a) Temperature dependence of the relative integrated PL intensity for $Ba_9Y_{1.94}Ce_{0.06}Si_6O_{24}$ (squares) showing a decrease of only 25% of room temperature quantum yield at 500 K, indicating this phosphor has thermal quenching properties on par with the industry standard, YAG:Ce^{3+} (circles).[3] (b) Minimal red shift and decrease in emission intensity observed for $Ba_9Y_2Si_6O_{24}:Ce^{3+}$ at temperatures below 295 K, whereas blue shift of the emission intensity is observed with increasing temperature.

the room temperature efficiency at 500 K. This small drop indicates this phosphor host is more thermally robust than many other silicates. For example, $M_2SiO_4:Eu^{2+}$ (M = Sr, Ba) decreases to 50% of room temperature efficiency around 400 K, which is much lower than the silicate presented here.[24] In fact, this phosphor has thermal quenching characteristics that approach the industry standard YAG:Ce^{3+}, which is also shown in Figure 7a.[3] The difference in thermal quenching properties likely arises from the connectivity of the compounds. For instance, the M_2SiO_4 phosphors contain isolated SiO_4 tetrahedral units that when excited have a greater degree of freedom, allowing for an increase in nonradiative relaxation via active phonon pathways. YAG:Ce^{3+} is fully connected with corner-shared tetrahedra−octahedra units that limit the vibrational degrees of freedom, improving the quenching characteristics. The connectivity in $Ba_9Y_{1.94}Ce_{0.06}Si_6O_{24}$ is closer to that of YAG:Ce^{3+}, containing corner-shared tetrahedra−octahedra. Even though $Ba_9Y_{1.94}Ce_{0.06}Si_6O_{24}$ only contains two-dimensional sheets rather than the three-dimensional connectivity of YAG:Ce^{3+}, it appears that even the two-dimensional connections make the lattice rigid enough to limit quenching of the phosphor. Because of these excellent thermal quenching characteristics, optimizing this phosphor to increase the room temperature PLQY will yield an excellent, thermally stable blue-green phosphor. In addition to the decrease in PLQY, there is a blue shift of approximately 15 nm with increasing temperature, illustrated in Figure 7b. This leads to CIE coordinates of (0.213, 0.306). As with the red shift in low temperature measurements, the higher temperatures cause an increase in the unit cell dimensions and corresponding Ce−O bond distances that decreases crystal field splitting.

$Ba_9(Y_{1-y}Sc_y)_2Si_6O_{24}:Ce^{3+}$ Solid Solution. Although $Ba_9Y_2Si_6O_{24}:Ce^{3+}$ is an efficient blue-green phosphor, device

dx.doi.org/10.1021/ic400614r | Inorg. Chem. 2013, 52, 8010−8016

integration would still require the addition of a red phosphor to improve color rendering. Alternatively, red-shifting $Ba_9Y_2Si_6O_{24}:Ce^{3+}$ could alleviate the need for an external red component. As was shown in $(Ba_{1-\delta}Sr_\delta)_9Sc_2Si_6O_{24}:Ce^{3+}$, Li^+, substituting the smaller Sr^{2+} for the larger Ba^{2+} leads to a substantial decrease in the lattice parameters, causing an increase in the crystal field splitting of the cerium ions, which red-shifted the emission spectra. Attempts to prepare a similar solid solution with yttrium (e.g., $(Ba_{1-\delta}Sr_\delta)_9Y_2Si_6O_{24}:Ce^{3+}$) did not lead to a formation of the desired phase and instead yielded a mix of Sr and Ba silicates. Thus, to red-shift the spectra, a solid solution following $Ba_9(Y_{1-y}Sc_y)_2Si_6O_{24}:Ce^{3+}$ (y = 0, 0.05, 0.1, ..., 0.25) was prepared. The Sc content (y) was limited to less than 25% because the absorption peak at 395 nm decreases beyond a point that would make this compound a viable near-UV excited phosphor. Performing a Rietveld refinement on these samples (y = 0.1 and 0.2; presented in Supporting Information) indicates the expected decrease in lattice parameters as the smaller Sc^{3+} is substituted for Y^{3+},[17] and there are only minor changes in the atomic positions. Substituting 10 and 20% of the scandium for yttrium in the structure leads to a respective unit cell volume decrease of ≈7 and 14 Å^3 compared to the volume of $Ba_9Y_2Si_6O_{24}$. Although this is a minor change in the volume, because Ce^{3+} is already squeezed on the Y/Sc−O site, this shortens the Ce−O bonds even more. As discussed in eq 2, the shorter bond distances lead to increased crystal field splitting and a red shift in the emission spectra, as is observed in parts b and d of Figure 8 for

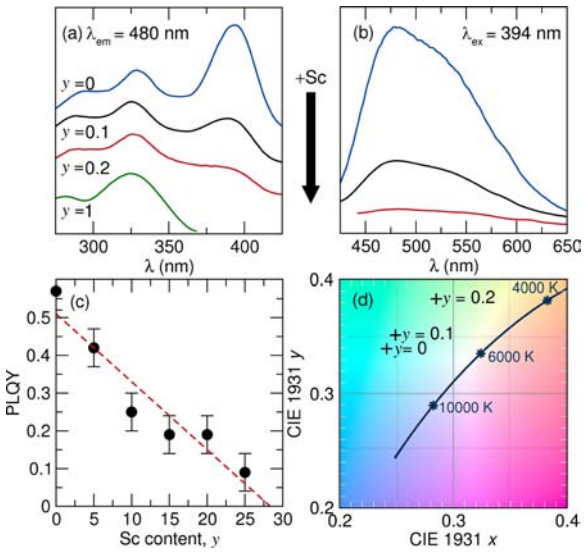

Figure 8. (a) Excitation spectra and (b) emission spectra for the solid solution of $Ba_9(Y_{1-y}Sc_y)_{1.94}Ce_{0.06}Si_6O_{24}$ showing the changes associated with the peak at λ_{max} = 394 nm. For comparison, $Ba_9Sc_2Si_6O_{24}$ is shown in green.[11] (c) PLQY decreasing almost linearly in the solid solution $Ba_9(Y_{1-y}Sc_y)_{1.94}Ce_{0.06}Si_6O_{24}$. (d) CIE color coordinates of $Ba_9(Y_{1-y}Sc_y)_{1.94}Ce_{0.06}Si_6O_{24}$ at room temperature showing the red shift of the emission peak with increasing Sc concentration.

y = 0.1 and 0.2. Although the desired red shift can be achieved by substituting Sc in a solid solution at relatively low substitution levels, y > 0.25, the $(Y/Sc)O_6$ pseudo-octahedral volume becomes too small for the larger Ce^{3+}, limiting substitution at the site. This is reflected in the excitation spectra for $Ba_9(Y_{1-y}Sc_y)_{1.94}Ce_{0.06}Si_6O_{24}$ (y = 0, 0.1, 0.2) as shown in Figure 8a. A sharp decrease in the intensity of the peak at 394 nm is observed as the concentration of Ce^{3+} decreases because of the volume constraints. A corresponding decrease in the observed emission intensity when this is excited at 394 nm (Figure 8b) arises because of the limited absorption. With the decrease in excitation/emission intensity, the PLQY decreases almost linearly from PLQY = 57% for the y = 0 to PLQY = 10% for y = 0.25. Although the desired red shift in the emission spectrum is achieved as indicated through CIE color coordinates, illustrated in Figure 8d, the substantial decrease in PLQY means careful optimization of the Ce^{3+} content and Sc^{3+} content will be required.

CONCLUSIONS

The identification of a novel barium yttrium silicate ($Ba_9Y_2Si_6O_{24}$) phase has provided a new host for a cerium-activated phosphor. The compound can be prepared as a nearly pure phase using conventional high temperature preparation methods, and the structure can be solved using synchrotron X-ray powder diffraction. It is isostructural with $Ba_9Sc_2Si_6O_{24}$ and contains SiO_4−YO_6−SiO_4 layers that stack along the [001] direction, forming infinite sheets. When Ce^{3+} is substituted in the structure, it occupies the Ba^{2+} and the Y^{3+} sites. The strong crystal field splitting of the pseudo-octahedral coordination environment leads to an excitation with a λ_{max} of 394 nm. When this peak is excited using near-UV light, an efficient (≈60%) blue-green emission is produced. Temperature-dependent measurements show a red shift in the emission spectra at 77 K due to the contraction of the unit cell at low temperatures. At elevated temperatures, the photoluminescence shows a decrease of only 25% at 500 K, outperforming many other Ce^{3+}-substituted silicate phosphors. Finally, a red shift in the emission spectrum can be achieved by increasing the crystal field splitting of the pseudo-octahedral site by decreasing the polyhedral volume through preparing the solid solution $Ba_9(Y_{1-y}Sc_y)_2Si_6O_{24}:Ce^{3+}$. Although a red shift is obtained, a decrease in the PLQY accompanies the Y^{3+}/Sc^{3+} mixing. Nevertheless, careful optimization of the Ce^{3+} content and Sc^{3+} concentration can lead to an ideal blue-green phosphor. These photoluminescent characteristics make this new cerium-substituted phosphor a good candidate to cover the blue-green portion of the visible spectrum, leading to a better white LED.

ASSOCIATED CONTENT

Supporting Information

The Rietveld refinement, crystallographic data, and figures of the corresponding fits for the Y−Sc solid solution, $Ba_9Y_{1.94}Ce_{0.06}Si_6O_{24}$ (y = 0, 0.1, 0.2). This material is available free of charge via the Internet at http://pubs.acs.org.

AUTHOR INFORMATION

Corresponding Author

*E-mail: jrbrgoch@mrl.ucsb.edu.

Notes

The authors declare no competing financial interest.

ACKNOWLEDGMENTS

The authors thank Megan Butala for assistance with the SEM. Fellowship support for K.A.D. from the ConvEne IGERT Program (NSF-DGE 0801627) is gratefully acknowledged. The research reported here made use of MRL Central Facilities, supported by the MRSEC Program of the NSF under Award

DMR 1121053. Use of the Advanced Photon Source at Argonne National Laboratory was supported by the U.S. Department of Energy, Office of Science, Office 27 of Basic Energy Sciences, under Contract DE-AC02-06CH11357.

REFERENCES

(1) Nakamura, S.; Fasol, G. *The Blue Laser Diode: GaN Based Light Emitters and Lasers*; Springer: Berlin, Germany, 1997.
(2) Xie, R.-J.; Hirosaki, N. *Sci. Technol. Adv. Mater.* **2007**, *8*, 588−600.
(3) Birkel, A.; Denault, K. A.; George, N. C.; Doll, C. E.; Hery, B.; Mikhailovsky, A. A.; Birkel, C. S.; Hong, B.-C.; Seshadri, R. *Chem. Mater.* **2012**, *24*, 1198−1204.
(4) Bachmann, V.; Ronda, C.; Meijerink, A. *Chem. Mater.* **2009**, *21*, 2077−2084.
(5) Park, J. K.; Choi, K. J.; Kang, H. G.; Kim, J. M.; Kim, C. H. *Electrochem. Solid-State Lett.* **2007**, *10*, J15−J18.
(6) Kim, J. S.; Park, Y. H.; Choi, J. C.; Park, H. L. *J. Electro. Soc.* **2005**, *152*, H135−H137.
(7) Denault, K. A.; George, N. C.; Paden, S. R.; Brinkley, S.; Mikhailovsky, A. A.; Neuefeind, J.; DenBaars, S. P.; Seshadri, R. J. *Mater. Chem.* **2012**, *22*, 18204−18213.
(8) Han, J. Y.; Im, W. B.; Kim, D.; Cheong, S. H.; Lee, G.-Y.; Jeon, D. Y. J. *Mater. Chem.* **2012**, *22*, 5374−5381.
(9) Nakano, T.; Kawakami, Y.; Uematsu, K.; Ishigaki, T.; Toda, K.; Sato, M. *J. Lumin.* **2009**, *129*, 1654−1657.
(10) Bian, L.; Zhou, T.; Yang, J.; Song, Z.; Liu, Q. *J. Lumin.* **2012**, *132*, 2541−2545.
(11) Brgoch, J.; Borg, C. K. H.; Denault, K. A.; DenBaars, S. P.; Seshadri, R. *Solid State Sci.* **2013**, *18*, 149−154.
(12) Larson, A. C.; Dreele, R. B. V. *General Structure Analysis System*; Los Alamos National Laboratory Report LAUR 86-748, 2000.
(13) Toby, B. H. *J. Appl. Crystallogr.* **2001**, *34*, 210−213.
(14) Greenham, N. C.; Samuel, I. D. W.; Hayes, G. R.; Phillips, R. T.; Kessener, Y. A. R. R.; Moratti, S. C.; Holmes, A. B.; Friend, R. H. *Chem. Phys. Lett.* **1995**, *241*, 89−96.
(15) Im, W. B.; Brinkley, S.; Hu, J.; Mikhailovsky, A.; DenBaars, S. P.; Seshadri, R. *Chem. Mater.* **2010**, *22*, 2842−2849.
(16) Wang, L. H.; Schneemeyer, L. F.; Cava, R. J.; Siegrist, T. *J. Solid State Chem.* **1994**, *113*, 211−214.
(17) Shannon, R. *Acta Crystallogr. A* **1976**, *32*, 751−767.
(18) Blasse, G. *Phys. Lett. A* **1968**, *28*, 444−445.
(19) Im, W. B.; Kim, Y.-I.; Kang, J. H.; Jeon, D. Y.; Jung, H. K.; Jung, K. Y. *J. Mater. Res.* **2005**, *20*, 2061−2066.
(20) Yao, S. S.; Xue, L. H.; Li, Y. Y.; You, Y.; Yan, Y. W. *Appl. Phys. B: Lasers Opt.* **2009**, *96*, 39−42.
(21) Rack, P. D.; Holloway, P. H. *Mater. Sci. Eng., R* **1998**, *21*, 171−219.
(22) Blasse, G.; Grabmaier, B. C. *Luminescent Materials*; Springer-Verlang: Berlin, Germany, 1994.
(23) da Silva, C.; de Araujo, M.; Gouveia, E.; Gouveia-Neto, A. *Appl. Phys. B: Lasers Opt.* **2000**, *70*, 185−188.
(24) Kim, J. S.; Jeon, P. E.; Choi, J. C.; Park, H. L. *Solid State Commun.* **2005**, *133*, 187−190.